Self-diffusion in dilute quasi-two-dimensional hard sphere suspensions: Evanescent wave light scattering and video microscopy studies

Andrew H. Marcus, Binhua Lin, and Stuart A. Rice
Department of Chemistry and The James Franck Institute, The University of Chicago, Chicago, Illinois 60637
(Received 24 August 1995)

We report measurements of the diffusion coefficient of a dilute quasi-two-dimensional hard sphere colloidal suspension using two independent experimental techniques: evanescent wave dynamic light scattering (EWDLS) and digital video microscopy (DVM). The system studied consists of 1 μm sterically stabilized, uncharged, poly(methylmethacrylate) spheres in a very thin cell (~ 3 μm). In principle, EWDSL and DVM yield identical information about the system, albeit by different analyses. When both methods are used to study the same system it is possible to directly compare measurements of preaveraged statistical dynamical quantities with their microscopic counterparts. Our EWDLS measurements yield the effective diffusion coefficient as a function of wave number and the mean square particle displacement, for fixed wave number, as a function of time. The DVM measurements generate particle trajectories; Fourier decomposition of the trajectories yields the dynamic scattering function, which is found to be in quantitative agreement with the same function measured by EWDLS. Analysis of the observed intermediate scattering function indicates that, as predicted by Cichocki and Felderhof [J. Phys. Condens. Matter **6**, 7287 (1994)], in this quasi-two-dimensional system the time dependence of the evolution of the effective diffusion coefficient from its short time value to its long time value has the form $(\ln t)/t$. To our knowledge, these results are the first experimental verification of the predicted temporal evolution of the diffusion coefficient for Brownian motion in a quasi-two-dimensional liquid.

PACS number(s): 61.20.−p

I. INTRODUCTION

The discovery of the very slow temporal decay of the velocity autocorrelation function of a fluid, by Alder, Gass, and Wainwright, fundamentally altered our understanding of the relationship between the contributions of local motion and collective motion to diffusion [1]. Studies of the asymptotic ($t \rightarrow \infty$) time dependence of the Green-Kubo integrands have established that so called long time tails are characteristic of all of the autocorrelation functions whose integrals define transport coefficients in a fluid. Moreover, the importance of the long time tail for a particular transport coefficient depends on the dimensionality of the system, and it has been known for more than 20 years that transport phenomena in a two-dimensional fluid are different from their three-dimensional counterparts.

The development of an improved theoretical understanding of transport phenomena in pure fluids has been paralleled by theoretical studies of Brownian motion in systems where the excluded volume and hydrodynamic interactions between a Brownian particle and the solvent and between Brownian particles cannot be neglected. As for the case of pure fluids, the time dependence of the effective diffusion coefficient of a Brownian particle is predicted to be different in two and three dimensions. It is found that the initial motion of an isolated Brownian particle induces a hydrodynamic flow field in the host liquid which recirculates around the particle and exerts a very slowly decaying force on it. In three dimensions the velocity autocorrelation function of an isolated Brownian particle has a long time tail which decays as $t^{-3/2}$, hence its diffusion coefficient is well defined in the limit $t \rightarrow \infty$. In two dimensions the velocity autocorrelation function of an isolated Brownian particle has a long time tail which decays as t^{-1}, hence its diffusion coefficient is undefined in the limit as $t \rightarrow \infty$. These results are consequences of the structures of the Liouville operators which determine the dynamical evolution of the three- and two-dimensional systems.

There has also been considerable development of a limiting version of the theory of Brownian motion for a time scale on which the hydrodynamic interactions can be treated as instantaneous. In this limit the divergent behavior of the two-dimensional diffusion coefficient is absent and the evolution of the system can be described by a generalized Smoluchowski equation. We shall refer to this model system as a Smoluchowski liquid. The diffusion coefficient in a Smoluchowski liquid has interesting properties. The value of the zero wave vector diffusion coefficient is time dependent by virtue of the difference between the two (Brownian) particle equilibrium distribution function and the two particle distribution function modified by the presence of a steady state flow. In the short time limit that diffusion coefficient is determined by an integral of hydrodynamic interaction functions weighted by the equilibrium two particle distribution function [2]. In the long time limit the value of that diffusion coefficient is determined by an integral of hydrodynamic interaction functions weighted by the radial part of the solution to the two particle Smoluchowski equation [3]. In a two-dimensional Smoluchowski liquid the asymptotic value for the diffusion coefficient of the

Brownian particle is reached very slowly. Indeed, Cichocki and Felderhof [4] predict that in a two-dimensional Smoluchowski liquid the temporal evolution of the diffusion coefficient from its short time value to its long time value has the form $(\ln t)/t$.

From a fundamental point of view, a Smoluchowski evolution operator cannot be used to describe diffusion dynamics in a two-dimensional suspension of Brownian particles because that operator implies that the hydrodynamic interactions in the system are instantaneous, hence the retardation effects associated with the long time tail of the velocity autocorrelation function are absent and the diffusion coefficient is finite. As mentioned at the beginning of this section, in a two-dimensional suspension whose dynamics are described by the Liouville operator the hydrodynamic motion of the host liquid induced by the Brownian particle leads to divergence of its diffusion coefficient. However, the use of the Smoluchowski evolution operator is appropriate, hence also the Cichocki-Felderhof analysis, for the description of a *quasi-two-dimensional* suspension of Brownian particles which we define with the following conditions. First, the vortex motion that generates the long time tail in the velocity autocorrelation function must be quenched. Second, the scale length for decay of in-plane momentum transfer correlations must greatly exceed that for out-of-plane momentum transfer correlations. Third, the range of the in-plane positional correlations must greatly exceed the range of the out-of-plane positional correlations. Fourth, the Brownian particle displacements transverse to the plane must be negligibly small.

An experimental realization of a strictly two-dimensional colloid suspension does not exist. It is possible, however, to design a system with characteristics that approach quasi-two-dimensional behavior as defined above. In this paper we describe the results of two independent measurements of diffusion in a dilute quasi-two-dimensional colloidal suspension consisting of sterically stabilized poly(methylmethacrylate) (PMMA) spheres in a cell whose thickness is only of order three times the particle diameter. Since the PMMA particles are uncharged the system can be accurately modeled as an assembly of hard spheres undergoing Brownian motion. In one sense the system we have studied has three-dimensional character. That is, both the ratio of the diameters of the Brownian particle and a solvent molecule (~ 500) and the space between a Brownian particle and the wall (~ 500 solvent molecule diameters) are sufficiently large that the flow of host liquid around a Brownian particle must be described as three dimensional. Therefore one cannot expect a suspension of the type we have studied to exhibit divergence of the Brownian particle diffusion coefficient. However, the system we have studied does approximate a quasi-two-dimensional suspension of Brownian particles since the walls of the cell impose boundary conditions on the flow of the host liquid induced by the motions of the Brownian particles which make the decay length for out-of-plane momentum transfer very small compared to the decay length for in-plane momentum transfer. We believe that the walls of our cell, which are coated with an alkane brush, prevent the propagation of vortices that are generated by motion of a Brownian particle and thereby quench the long time tail of the velocity autocorrelation function. We note that the boundary conditions also increase the frictional force that impedes the in-plane Brownian motion, hence decease the diffusion coefficient of an isolated Brownian particle. Finally, the motions of the centers of the Brownian particles are observed to be in plane to within a small fraction of a particle diameter, hence the excluded volume interaction of the particles is entirely in the plane of the particle centers.

The two experimental methods we have used are evanescent wave dynamic light scattering (EWDLS) and digital video microscopy (DVM). Our EWDLS measurements yield the effective diffusion coefficient as a function of wave number and the mean square particle displacement, for fixed wave number, as a function of time. The DVM measurements generate particle trajectories; Fourier decomposition of the trajectories yields the dynamic scattering function, which is found to be in quantitative agreement with the same function measured by EWDLS. Analysis of the observed intermediate scattering function indicates that, as predicted by Cichocki and Felderhof, in this quasi-two-dimensional system the time dependence of the evolution of the effective diffusion coefficient from the free Brownian particle value to the interaction dressed value has the form $(\ln t)/t$. To our knowledge our results are the first experimental verification of the predicted temporal evolution of the diffusion coefficient for Brownian motion in a quasi-two-dimensional liquid.

II. THE MODEL SYSTEM

The system we have studied consists of 1 μm diameter spherical PMMA particles in a very thin cell (~ 3 μm). The surface of each PMMA particle was covered with a ~ 20 Å oligomeric brush of poly(3-hydroxystearate) that acts to sterically stabilize it with respect to aggregation induced by van der Walls forces. The PMMA particles were suspended in an aqueous sucrose solution (10% by weight) that is confined between the walls of a thin glass cell. The cell walls were coated with trihydroxyoctadecylsilane, which acts to prevent adsorption of PMMA particles to the wall. The spacing between the cell walls could be varied and, for the experiments reported, was set to approximately three particle diameters. We determined, by direct microscopic examination, that this thin cell configuration constrained the PMMA particle centers to a plane within a small fraction of a particle diameter.

Monodisperse 1 μm PMMA spheres, synthesized according to the method of Ottewill and co-workers [5], were obtained from the Seradyne Corporation. The particles were washed free of any surfactant impurities by repeated sedimentation followed by resuspension in purified water (Nanopure system, 18 MW, with a 0.2 μm filter). The particles were then resuspended in 10% (by weight) aqueous sucrose solution (Fisher Scientific).

A schematic diagram of the thin cell used in both experiments is shown in Fig. 1. Cells were constructed

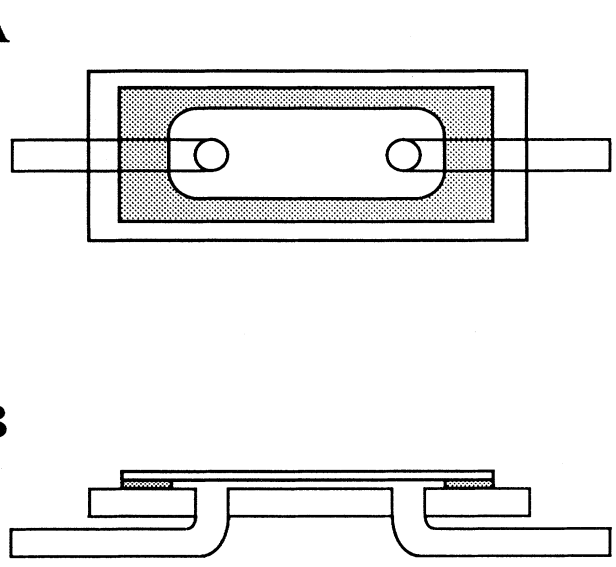

FIG. 1. Schematic of experimental cell for thin colloidal suspensions. (A) Top view. (B) Side view. One glass microscope slide, one glass cover slip, and two bent pieces of glass tubing are joined together with epoxy to form airtight seals. The shaded area represents the region between the cover slip and the microscope slide that is filled with epoxy. The cell is charged with sample through the tubing. The tubing is made part of a closed manifold system which may be pumped out to adjust the sample out-of-plane dimension.

from glass microscope slides, No. 1 microscope cover slips (0.18 mm thickness), and glass tubing (outer diameter equal to 4 mm). Two $\frac{1}{8}$ in. holes separated by $\frac{3}{4}$ in. were drilled through the microscope slides. All glass surfaces were then treated with an octadecylsilicone coating (Glassclad 18, United Chemical Products). The glass tubing was sealed to the slides using a nonleaching epoxy that wets glass well (Epo-tek 302 3M, Epoxy Technologies, Inc.). Before its application, the epoxy was degassed in a vacuum dessicator. All parts were oven baked ($T=85\,^{\circ}$C) overnight to assist in the curing process. The cover slips were glued to the opposite slide surface using an epoxy that cures when exposed to ultraviolet light (Norland UV epoxy, Norland Productions, Inc.). The gluing was accomplished by drawing a thin line of the epoxy along the inside edge of the cover slip, then lowering the glass slide onto the cover slip. Immediately after contact was made between the surfaces, the glue was cured by exposure to a 100 W UV lamp source. The cells were allowed to further cure at an elevated temperature overnight ($T=85\,^{\circ}$C).

The finished cells were charged with sample in a sequential manner. First, purified water was introduced, followed by 10% sucrose solution, and finally the PMMA suspension. The glass tubing was attached to a manifold system constructed from tygon tubing and a Nalgane vacuum hand pump (Fisher Scientific). By the application of a slight vacuum, it is possible to adjust the inner wall spacing between the slide and coverslip. It was found that wall spacings between 10 and 3 μm (measured by microscopy) were easily achieved.

Samples were observed under the microscope to determine if a quasi-two-dimensional suspension was formed, the criteria being that the particle centers lie in a plane and that motion out of the plane is suppressed. Such samples could usually be made when the wall spacing was reduced to 3 μm. Light scattering and microscopy measurements were made on the same sample.

For the EWDLS experiments, the scattered light intensity was detected using a single-mode optical fiber with a grin lens mounted on both ends (Fujikura, Japan). The detection end was mounted on a rotation stage able to rotate around the axis of the cell with an in-plane precision $\pm 0.5^{\circ}$. The distance between the lens and the illumination area was approximately 50 cm with an out-of-plane angle $\psi''' = 5^{\circ}$. The illumination area was visible to the fiber through a 2 mm circular pinhole in a mask placed flush over the outer cell surface. The mask considerably decreases the detection of stray light arising from multiple reflections in the cell. The detection of stray light was further decreased by the small acceptance angle of the optical fiber ($\leq 0.5^{\circ}$). The transmitting end of the fiber was joined to a photomultiplier tube. The temporal intensity autocorrelation function was obtained using a digital correlator (BIAT9000, Brookhaven Instruments). The excitation source was a 100 mW Coherent argon ion laser; its output power was typically set to 30 mW.

The DVM measurements were made using an Olympus BH2 metallurgical microscope with a 100×, numerical aperture 1.2, oil immersion objective. The objective's depth of focus is a fraction of the PMMA sphere diameter, so that nonplanar particle configurations were easily detected. Images of the suspension were captured by a Hitachi charge coupled device (CCD) video camera mounted to the camera eyepiece. The frame speed of the CCD was 30 Hz, while its shutter speed was $\frac{1}{100}$ of a second. The analog camera output was sent directly to the video port of a Silicon Graphics Indy (SGI) workstation. The SGI frame grabber supplied with the workstation was used to digitize sequences of 320×240 square pixel frames. A typical run consisted of 100 frames in sequence, corresponding to roughly 25 Mbytes of data. All image processing procedures were implemented using IDL (Research Systems, Inc.), a programming language optimized for visual data analysis. The pixel length was calibrated by imaging a transmission electron microscope (TEM) grid of known scale. The aspect ratio was determined to be 1 ± 0.1 and the calibrated pixel dimension was 1 pixel $=0.174\pm 0.0015$ μm.

III. BACKGROUND INFORMATION

In order to discuss the qualitative behavior of the transport properties of a coloidal suspension, it is necessary to define some characteristic time constants. As described by Tokuyama and Oppenheim [6], there are five pertinent characteristic times associated with any hard sphere suspension: the relaxation time of the velocity autocorrelation function of the solvent molecules, t_0; the

momentum relaxation time of fluid displaced by a particle's volume, τ_f; the relaxation time of the velocity autocorrelation function of the Brownian particle, τ_B; the time after which hydrodynamic effects become important, τ_H; and the structural relaxation time τ_D during which particles diffuse a hydrodynamic screening length l. In the case of dilute colloidal suspensions, where the Brownian particle mass density is not very different from the fluid mass density, the relative time scales can be arranged as follows: $t_0(\text{ps}) \ll \tau_f(\text{ns}) \sim \tau_B(\text{ns}) \ll \tau_H(\text{ms}) \ll \tau_D(\text{s})$.

A theoretical prediction of the time-dependent effective self-diffusion coefficient for a two-dimensional Smoluchowski suspension of Brownian disks, $D_S(t)$, has been worked out by Cichocki and Felderhof [4]. When t is large relative to τ_D, the mean square displacement of a given particle increases linearly with time. This asymptotic behavior defines the long time self-diffusion constant D_S^L. The value of D_S^L depends on steady state hydrodynamic conditions such as interparticle and particle-wall interactions as well as the particle concentration. These boundary conditions also determine the functional form of the evolution of $D_S(t)$ from its initial value, D_S^S, to D_S^L. It is a consequence of the two-dimensional boundary condition that $D_S(t)$ tends to D_S^L very slowly. This evolution is detectable at intermediate times $\tau_H < t < \tau_D$ and, accounting for particle interactions, is predicted to have the peculiar behavior $D_S(t) \sim A + B(\ln t)/t$, where A and B are constants. We review the basis for this prediction later in this section.

As mentioned in Sec. I, we have employed two independent, yet complementary, methods to study quasi-two-dimensional Brownian motion. The first, evanescent wave dynamic light scattering is a direct measurement of the time autocorrelation function of intensity fluctuations of in-plane scattered light [7–9]. The scattering excitation source is an evanescent wave that propagates parallel to and within the sample plane. This evanescent wave is produced by the total internal reflection of a monochromatic beam that is directed from within the glass wall of the experimental cell toward its dielectric interface with the colloid suspension. The amplitude of the evanescent wave decays exponentially with distance from the interface with a decay constant on the order of the excitation wavelength ($d_p \sim \lambda_{\text{ex}}$). Thus, in applying the EWDLS geometry to the thin cell configuration described above, the time correlation of the scattered light intensity is directly related to the collective in-plane motions of the colloid particles. An important aspect of this measurement is that it is sensitive to the motions of macroscopic numbers of particles and, for this reason, is representative of an ensemble averaged dynamical quantity [10]. The experimental observable is therefore simply related to the two-dimensional dynamic scattering function. Recently, EWDLS has been successfully applied to the measurement of diffusion of disklike diblock copolymer aggregates adsorbed at the air-water interface [8,9].

The second method we have used is digital video microscopy [11–14]. Unlike EWDLS, a combination of DVM, sophisticated image processing, and computer tracking algorithms can be used to obtain individual particle coordinates as an explicit function of time. The methodology for performing all three tasks with optimized precision is still evolving [15]. In principle, it is a straightforward, though numerically taxing, application of statistical mechanics to calculate the ensemble averaged two-dimensional dynamic scattering function from the N particle trajectories.

The DVM data provide a direct representation of the two-dimensional Brownian particle dynamics, while the light scattering measurements lead to time correlation functions that already contain preaveraged microscopic dynamical information. By examining the consistency between these results, it is possible to test the validity of either method over the range of temporal and spatial parameters that the two have in common.

To provide the reader with an understanding of the predicted temporal evolution of the diffusion coefficient for two-dimensional Brownian motion in a Smoluchowski liquid we briefly review the work of Cichocki and Felderhof [4]. They consider a system of N identical circular disks undergoing Brownian motion in a plane. The particles have radii a and are confined to an area Σ by a wall potential. The "free particle" diffusion coefficient is given by the constant D_0. The motion of a labeled particle is affected by particle-particle interactions. The configuration of the system is specified by the $2N$-dimensional vector $\mathbf{X}=(\mathbf{R}_1, \ldots, \mathbf{R}_N)$, where the components of the vector $\mathbf{R}_i$ are the Cartesian coordinates of the ith disk. The time dependence of $\mathbf{X}$ is characterized by the solution to the generalized Smoluchowski equation, $P(\mathbf{X},t)$, which is the conditional probability that the system will adopt the configuration $\mathbf{X}$ at time t given the initial condition [10]. In the long time limit $P(\mathbf{X},t)$ approaches the Boltzmann distribution, $P_{\text{eq}}(\mathbf{X}) = \exp[-\beta\Phi(\mathbf{X})][Z(\beta)]^{-1}$, where $\beta=(k_B T)^{-1}$, $\Phi(\mathbf{X})$ contains both wall and particle interactions, and $Z(\beta)$ is the canonical partition function. The solution is taken in the thermodynamic limit ($N \to \infty, \Sigma \to \infty, \rho = N/\Sigma$) [10].

The self-diffusion coefficient is defined in terms of the mean square displacement of a labeled particle, $W(t) = \langle [\mathbf{R}_1(t) - \mathbf{R}_1(0)]^2 \rangle /4$, and can be written as

$$D_S(t) = D_S^L + \mu_S(t) , \tag{3.1}$$

where the relaxation function $\mu_S(t)$ is related to the memory function $M_S(t)$ through

$$\mu_S(t) = -\int_t^\infty M_S(t')dt' . \tag{3.2}$$

The memory function is defined as the ensemble averaged autocorrelation of the fluctuating force experienced by the particles [10]. For the treatment given by Cichocki and Felderhof [4], the evolution of $M_S(t)$ is due completely to particle-particle collisions. The relaxation function describes the evolution of the diffusion coefficient to its asymptotic limit D_S^L. For two-dimensional Smoluchowski systems $\mu_S(t)$ is expected to decay on a time scale comparable to τ_D.

Since the self-diffusion coefficient is related to the mean square displacement through $D_S(t) = dW(t)/dt$, Eq. (3.1)

can be integrated to obtain

$$W(t)=D_S^L t+\int_0^t \mu_S(t')dt' \ . \tag{3.3}$$

By solving the Smoluchowski equation for two interacting hard disks, Ackerson and Fleishman have shown that for a semidilute two-dimensional system of Brownian particles $\mu_S(t)$ decays as $1/t$ in the time range $\tau_H < t < \tau_D$ [16]. This result was used by Cichocki and Felderhof to obtain [4]

$$W(t)=D_S^L t+(D_S^S-D_S^L)\tau_L \ln(t/\tau_M)+o(1) \ , \tag{3.4}$$

where τ_L and τ_M are, respectively, "long" and "medium" scale time constants. It is apparent from Eq. (3.4) that the logarithmic correction to the diffusive behavior of the mean square displacement can only be important during times of order τ_M and for $(D_S^S-D_S^L)$ significantly greater than zero.

The logarithmic term in Eq. (3.4) can be detected experimentally if one considers an effective self-diffusion coefficient defined by the ratio $\tilde{D}_S(t)=W(t)/t$. Making use of this definition and Eq. (3.4),

$$\tilde{D}_S(t)=D_S^L+(D_S^S-D_S^L)\tau_L\left[\frac{\ln(t/\tau_M)}{t}\right]+o(1) \ . \tag{3.5}$$

Equation (3.5) describes the long time asymptotic behavior of the diffusion coefficient. The $(\ln t)/t$ functional form is predicted to be independent of particle interactions, at least for the case of short range interactions, and is a signature of the solution to the two-dimensional Smoluchowski equation with direct particle-particle interactions.

IV. EXPERIMENTAL OBSERVABLES AND DYNAMIC QUANTITIES

The EWDLS method has been previously described in detail by Lin and Rice [8], while the DVM methodologies are reviewed in an article by Crocker and Gier [15]. Nevertheless, there are important distinctions between the previously studied experimental systems and the one we have studied. For this reason, it is necessary to discuss some of the details of our applications of these methods in order to place them into a proper context.

A. Dynamic light scattering

In EWDLS measurements, the experimental observable is the time correlation function (the intermediate scattering function) that reflects the growth and decay of fluctuations in a spatial Fourier component of the refractive index with wavelength $2\pi Q^{-1}$, where Q (defined below) is the scattering wave vector. Roughly speaking, the decay time associated with a particular value of Q is given by $\tau_0=[D_0Q^2]^{-1}$, which is the time required for a noninteracting particle to diffuse the distance Q^{-1}. The range of Q probed is significant when compared to the mean separation between the particles, $L=\rho^{-1/2}$. The hydrodynamic regime corresponds to small-Q measurements ($Q^{-1} \gg L$) that probe collective large scale motions occurring on the relatively long time scale ($\tau_0 \sim \tau_D$). Large-Q measurements probe small scale, short time motions of individual particles ($Q^{-1} \ll L$ and $\tau_0 \ll \tau_D$). The latter is referred to as the microscopic regime. For the semidilute systems examined in this work, the area fraction $\eta=\rho\pi a^2 \cong 0.01$, $L \cong 8.5$ μm and 0.07 $\mu m \leq Q^{-1} < 0.2$ μm, so that our EWDLS measurements probe the microscopic dynamics of individual particles.

We show in Fig. 2 a schematic representation of the EWDLS experimental geometry we have used. The continuous wave emission of an argon ion laser ($\lambda_{ex}=5145$ Å) is used as the radiation source. The beam propagates within the x-z plane and is incident on a hemispherical glass lens upon which rests the experimental cell. The angle of incidence θ_i is set to a value larger than the critical angle for total internal reflection [which depends on the relative refractive index at the dielectric interface, $\theta_c=\arcsin(n_c)$, where $n_c=n_2/n_1$ and $n_2<n_1$]. Index matching fluid ($n_1=1.52$) is used to join the glass surfaces between the cell and lens. Total internal reflection occurs at the interface between the colloid suspension and the inner cell wall. Since the latter surface is coated with an 18 carbon amphiphile, the value of n_2 is taken as an average between that of 10% sucrose solution ($n=1.38$) and octadecane ($n=1.44$) such that $n_2 \approx 1.41$ and $\theta_c \approx 68^\circ$. The spatial dependence of the evanescent wave contained in the x-z plane is given by [8]

$$E_{EW} \propto \exp(-iQ_{EW}x-d_p z) \ , \tag{4.1}$$

where

$$Q_{EW}=\frac{2\pi n_1 \sin\theta_i}{\lambda_{ex}} \tag{4.2}$$

and the penetration depth is

$$d_p=\frac{\lambda_{ex}}{2\pi n_1(\sin^2\theta_i-n_c^2)^{1/2}} \ . \tag{4.3}$$

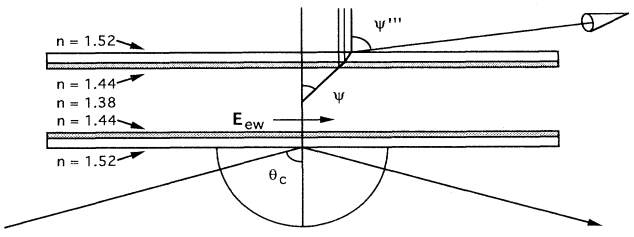

FIG. 2. Schematic representation of the EWDLS geometry. The excitation laser beam ($\lambda_{ex}=5145$ Å) is directed through a hemispherical glass lens towards the sample cell surface at the angle $\theta_c=68^\circ$. The evanescent wave $\mathbf{E}_{EW}$ propagates parallel to the sample plane in the same direction incidence. The shaded areas represent the 18 carbon coating on the inner glass surfaces. The refractive index n of each surface is shown. The out-of-plane detector position is defined by the angle ψ'''. This determines the out-of-plane scattering angle ψ.

Substitution of the above values and $\theta_i = 70^\circ$ into Eqs. (4.2) and (4.3) leads to $Q_{EW} = 1.74 \times 10^5$ cm^{-1} and $d_p \cong 0.36$ μm. Although the particles are located in a plane parallel and approximately 1.5 μm above the x-y plane, the magnitude of the evanescent wave field [$\sim 6\%$ as given by Eq. (4.1)] is still large enough to generate measurable scattering.

The incident evanescent wave propagates along the x direction and scatters from the particles suspended in the fluid. The subsequent change in photon momentum in the x-y plane results in an azimuthal- and polar-angle-dependent in-plane scattering wave vector given by [8]

$$Q_{xy} = (1 - 2\cos\psi\cos\phi + \cos^2\psi)^{1/2} , \tag{4.4}$$

where ϕ is the azimuthal (in-plane) scattering angle and ψ is the polar (out-of-plane) angle. In order to reach the detector, the scattered evanescent wave must pass through the top portion of the cell. As the scattered light passes through this interface, subsequent refraction leads to a larger value of ψ. If the coating on the glass wall is accounted for, there are three dielectric interfaces that the scattered light must pass through; suspension to coating, coating to glass, and glass to air. A simple application of Snell's law can be used to perform the three stage transformation from ψ to ψ''' (see Fig. 2). One finds

$$\psi = \arcsin\left[\frac{n'''\sin\psi'''}{n}\right] . \tag{4.5}$$

In Eq. (4.5), ψ''' is the polar angle of the scattered evanescent wave after it has passed through the final interface before it reaches the detector, n''' is the refractive index of air ($n''' = 1.0$), and n is the refractive index of the sucrose solution. Typically, the value of ψ''' is fixed by the out-of-plane placement of the detector while measurements are made for various values of the in-plane angle ϕ. The ϕ component of Q_{xy} is assumed to be unaffected by refraction through the cell. Therefore Eqs. (4.4) and (4.5) can be used to calculate Q_{xy} for a particular detector position. Table I lists values of ϕ and Q_{xy} used in the experiments presented here based on the value $\psi''' = 85.0^\circ$, leading to $\psi = 46.2^\circ$.

We make the standard assumptions used in dynamic light scattering; the scattering volume contains a large number of particles so that the amplitude of the scattered electric field is a Gaussian random variable; the background scattering is negligible compared to that due to the particles; and the suspension is sufficiently transparent that multiple scattering events are unimportant. Provided that these are accurate assertions, the time-dependent intensity autocorrelation function $g^{(2)}(t)$ as seen by the detector is given by [17]

$$g^{(2)}(Q,t) = \langle n \rangle^2 \{1 + f(A)[g^{(1)}(Q,t)]^2\} , \tag{4.6}$$

where $\langle n \rangle^2$ is the average number of photons counted during the experimental sampling time interval, $f(A)$ is a spatial coherence factor that depends on the time averaged number of coherence areas visible, and $g^{(1)}(Q,t)$ is the electric field temporal autocorrelation function [10]

$$g^{(1)}(Q,t) = \frac{\langle E(Q,0)E^*(Q,t)\rangle}{\langle |E(Q)|^2 \rangle} . \tag{4.7}$$

In Eqs. (4.6) and (4.7), Q is the in-plane scattering wave vector defined by Eq. (4.4) where the xy subscript has been omitted for clarity. For the remainder of this paper Q will refer to the in-plane component of the scattering wave vector.

Equation (4.6) describes the experimentally detected observable which is easily inverted to obtain $g^{(1)}(Q,t)$. $g^{(1)}(Q,t)$ is related to the intermediate scattering function through

$$g^{(1)}(Q,t) = \frac{F(Q,t)}{S(Q)} . \tag{4.8}$$

Comparison between Eqs. (4.7) and (4.8) shows that the static structure factor $S(Q)$ is the time averaged scattering intensity for a particular wave number, while the intermediate scattering function $F(Q,t)$ is the temporal autocorrelation function of the scattered field amplitude without normalization. The intermediate scattering function can be written as an explicit function of particle positions,

$$F(Q,t) = N^{-1} \sum_i \sum_j \langle \exp\{i\mathbf{Q}\cdot[\mathbf{R}_i(0) - \mathbf{R}_j(t)]\}\rangle , \tag{4.9}$$

where the zero time limit of Eq. (4.9) is defined as the static structure function

$$S(Q) = \lim_{t\to 0} F(Q,t) = N^{-1} \sum_i \sum_j \langle \exp[i\mathbf{Q}\cdot(\mathbf{R}_i - \mathbf{R}_j)]\rangle , \tag{4.10}$$

which serves to normalize the temporal decay given in Eq. (4.8). The structure function may also be related to the two-dimensional radial distribution function [18]

$$S(Q) = 1 + 2\pi\rho \int_0^\infty dr\, r g(r) J_0(Qr) , \tag{4.11}$$

where

$$J_0(x) = \frac{1}{2\pi} \int_0^{2\pi} d\theta \exp(ix\cos\theta) \tag{4.12}$$

is the zeroth-order Bessel function of the first kind [19].

Since we are interested in high-Q measurements applied to semidilute systems, rapid oscillations of the Bessel function in Eq. (4.11) cause the second term to

TABLE I. In-plane scattering wave numbers Q_{xy} for EWDLS measurements. ϕ is the in-plane scattering angle, Q_{xy} is given by Eq. (4.4), and $\tau_0 = [D_0 Q_{xy}^2]^{-1}$ is the approximate decay time of the self intermediate scattering function $F_S(Q,t)$. ($D_0 = 2.32 \times 10^{-9}$ cm^2 s^{-1}.)

ϕ (degrees)	Q_{xy} (cm^{-1})	Q_{xy}^{-1} (μm)	τ_0 (ms)
5	54 551	0.1833	145
30	91 128	0.1097	51.9
45	123 076	0.0813	28.5
55	144 026	0.0694	20.8

vanish, leaving $S(Q)=1$. Similarly, because $QL \gg 1$, the cross terms in Eqs. (4.9) and (4.10) do not contribute to their respective sums, leaving only the self terms. This again results in $S(Q)=1$ from Eq. (4.10), while Eq. (4.9) reduces to [17]

$$F_S(Q,t)=\langle \exp\{i\mathbf{Q}\cdot[\mathbf{R}(0)-\mathbf{R}(t)]\}\rangle , \tag{4.13}$$

where $F_S(Q,t)$ is the self part of the intermediate scattering function.

To relate Eq. (4.13) to the time-dependent diffusion coefficient, we employ the Gaussian model for single particle motion [17]. The Gaussian model makes use of the fact that the time scale associated with observation of the particle displacements is large compared to τ_B. In this case, $[\mathbf{R}(0)-\mathbf{R}(t)]$ may be treated as a Gaussian random variable which leads Eq. (4.13) to take the following form for two dimensions:

$$\begin{aligned} F_S(Q,t)&=\exp\left[-\frac{Q^2}{4}\langle[\mathbf{R}(0)-\mathbf{R}(t)]^2\rangle\right] \\ &=\exp[-Q^2W(t)] \\ &=\exp[-Q^2\tilde{D}_S(t)t] , \end{aligned} \tag{4.14}$$

where $W(t)$ is the two-dimensional mean square displacement given by Eq. (4.4) and $\tilde{D}_S(t)$ is the effective diffusion coefficient given by Eq. (4.5).

It is important to note that Eq. (4.14) represents a "first cumulant" approximation to the intermediate scattering function [10]. In general, the departure of $F_S(Q,t)$ from Gaussian behavior in Q will be reflected in the growing importance of the higher-order cumulants. There is theoretical evidence [20] that suggests the higher cumulants in dilute three-dimensional hard sphere suspensions are small. It is unclear whether the same result will hold for two dimensions. Nevertheless, it is shown below that Eq. (4.14) is an excellent approximation for the description of semidilute two-dimensional suspensions over a time scale on the order of the decay of the memory function ($\tau_B < t < \tau_D$).

The detection system used in our EWDLS measurements was operated in single photon counting mode. Photon counting rates were maintained around 10^5 s^{-1}, which was low enough that dead time effects are unimportant while the counting statistics are reasonably good. The scattered light detected by the optical fiber was nearly coherent so that $f(A)$ always had a value of at least 0.8. The time correlator had 239 channels. The experimental sampling time was 0.5 μs and the measured delay intervals ranged between 0.5 μs and 100 s. Data sets were accumulated in 300 s intervals. The number of photon counts in the first channel was typically 3×10^9. Individual data sets were normalized according to the measured average intensity [$\langle|E(Q)|^2\rangle$ in Eq. (4.7)], cross checked for consistency and then averaged together.

B. Digital video microscopy

Unlike EWDLS, the observable in a DVM experiment is a complete set of two-dimensional N particle trajectories,

$$C(\mathbf{R},t)=\sum_{i=1}^{N}\delta[\mathbf{R}-\mathbf{R}_i(t)] . \tag{4.15}$$

In DVM the minimum sampling time interval is determined by the time step between consecutive configurations. The experimental procedure is to image a representative area of the two-dimensional suspension onto the detector face of a high resolution CCD video camera. The analog video signal is subsequently converted into storable digitized information using a frame grabber. The process of transforming the information contained in a sequence of digitized images into the time-dependent density profile described by Eq. (4.15) is given by a prescription involving five logical steps. Here we provide a rough outline of the procedure; a more detailed description is given in an article by Crocker and Grier [15].

(i) Image restoration: The raw data images usually contain various defects that hinder immediate analysis. These include long wavelength contrast gradients and random pixel noise. The background artifacts are nominally due to uneven illumination or sensitivity of the camera pixels, while pixel noise is associated with the instrument response of the CCD camera and the frame grabber. Since pixel noise is nearly random with a correlation length λ_n equal to one pixel, it is greatly reduced by convolving the raw data image with a Gaussian surface of half-width λ_n. This operation suppresses the noise without noticeably decreasing the contrast. The resulting "noise reduced" image is further enhanced by subtracting off the "background" image. This "background" is constructed by performing a boxcar average of the raw data with a step size equal to $2w+1$, where w is the apparent sphere radius measured in pixels. The end result is an estimate of an "ideal" image that can be further processed.

(ii) Location of particle positions: The filtered images are analyzed to determine the locations of local brightness maxima. A pixel position is designated as a local maximum if one other pixel within a distance w has a larger value. Typically, the number of candidate local maxima found is larger than the number of particles in the frame. Since the maxima corresponding to the particle positions are the brightest of those found, only the brightest 30% of the candidates are accepted.

(iii) Refining candidate positions: The local maximum algorithm described by steps (i) and (ii) is sufficient to resolve particle positions to within half a pixel. The spatial resolution is improved by calculating the brightness weighted centroid positions from the spatial integral of circular areas with radius w centered at the original uncorrected positions. This correction is smaller than 0.5 pixel and has the overall effect of improving the resolution to 0.1 pixel.

(iv) Candidate particle discrimination: In addition to the integrated brightness within a circular area of radius w centered about each candidate position (m_0), the second moment of the brightness distribution (m_2) is also calculated. It is found that particle and nonparticle candidates form two distinct well separated distributions in the (m_0,m_2) plane. The candidates corresponding to the

true particle positions are selected based on this criterion.

(v) Linking sequential configurations into particle trajectories: In this final step it is necessary to determine which particle positions in a given image correspond to subsequent positions in later images. For dilute suspensions, the mean separation is much larger than single particle displacements, which are typically much smaller than the dimension of a particle. Therefore all trajectory displacements of interest are easily identified since they fall within an empirically determined cutoff range.

In principle, it is possible to calculate $F(Q,t)$ directly from the trajectory data given by Eq. (4.15). This may be accomplished in two ways. First, we consider the microscopic definition

$$F(Q,t)=\langle A_{-Q}(0)A_Q(t)\rangle \ , \tag{4.16}$$

where $A_Q(t)$ is the Fourier transform of the spatial particle density [Eq. (4.15)] given by

$$A_Q(t)=\left[\frac{1}{N}\right]^{1/2}\int d\mathbf{R}\exp(-i\mathbf{Q}\cdot\mathbf{R})C(\mathbf{R},t) \ . \tag{4.17}$$

For nonzero Q the combination of Eqs. (4.17), (4.15), and (4.16) results in an expression for $F(Q,t)$ that is an explicit function of $\mathbf{R}(t)$ given by the statistical average Eq. (4.9). This expression may be evaluated numerically using standard computer simulation techniques [21]. The effect of finite frame size is circumvented by employing a periodic boundary condition. Alternatively, image processing algorithms may be used to calculate $F(Q,t)$ from "idealized" images constructed from the particle trajectories. These ideal images are numerically Fourier transformed in two dimensions using standard fast Fourier transform (FFT) algorithms. Equation (4.16) is evaluated by calculating the time autocorrelation function of the Fourier space images for a particular time interval, averaged over many particle configurations.

Using these two independent methods of evaluating $F(Q,t)$ from the microscopic data, it is possible to check for self-consistency of the results for a single set of particle trajectories. Furthermore, it is possible to examine the differences between the full intermediate scattering function and the self part, $F_S(Q,t)$. As discussed in Sec. IV A, neglecting the cross terms ($j\neq i$) in Eq. (4.9) leads to an expression [Eq. (4.13)] for $F_S(Q,t)$. For the microscopy data presented in this work, the particle concentrations are small enough that the self and full intermediate scattering functions are indistinguishable by the methods described above. Therefore the previous assertion that these measurements correspond to the microscopic regime is experimentally verified.

V. RESULTS

In Fig. 3 we show a single restored image frame taken from a DVM data set and its associated trajectories. The pathways taken by individual particles appear to be unbiased by the possible presence of net solvent flow in the sample cell or transverse interactions with defects in the walls. This assertion was tested by constructing histograms of mean square displacements for all N particles as a function of time (see Fig. 4) and observing that the resulting spatial probability distributions are well modeled as Gaussian functions with a mean value equal to zero. These distributions are the self part of the van Hove function, $G_S(\mathbf{R},t)$, which is the time-dependent conditional probability that a particle will suffer a displacement $\mathbf{R}(t)$ from an initial position $\mathbf{R}(0)$ [17]. The time step between consecutive frames is 33 ms, so that the time correlation functions calculated from these trajectories are valid in the range ($\tau_H<t<\tau_D$). For the shortest time step, 33 ms, there are slight deviations of $G_S(\mathbf{R},t)$ from Gaussian behavior. These deviations become less visible as the time increment is increased.

The exact relationship between the van Hove function and the intermediate scattering function is given by a spatial Fourier transform.

$$F_S(Q,t)=\int_{-\infty}^{\infty}d\mathbf{R}\,G_S(\mathbf{R},t)\exp(i\mathbf{Q}\cdot\mathbf{R}) \ . \tag{5.1}$$

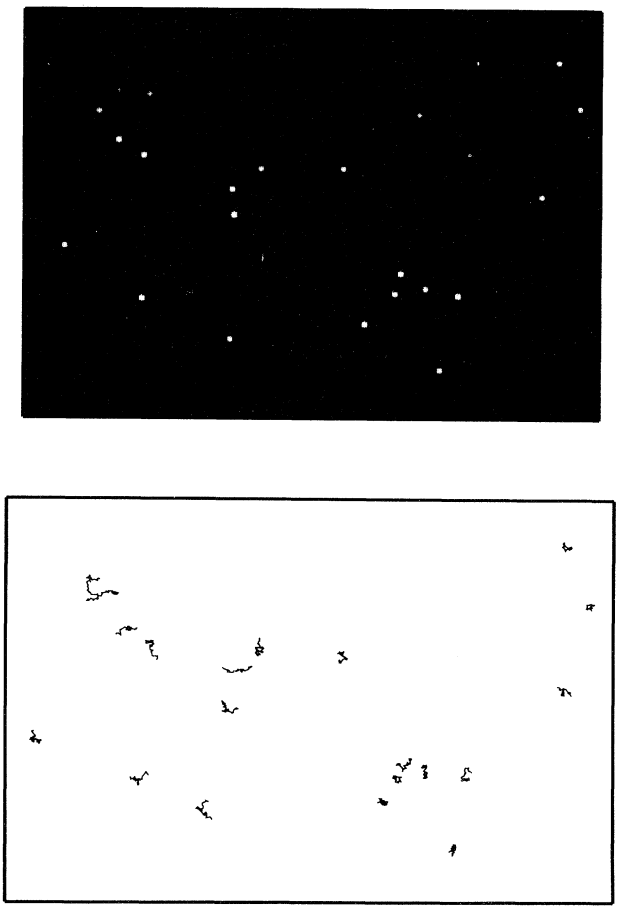

FIG. 3. Processed image of a quasi-two-dimensional colloidal suspension. The processing details are described in Sec. IV B. The two-dimensional packing density is approximately 1%. Shown below are individual center of mass particle trajectories for 30 consecutive image frames. The time interval between frames is 33 ms.

Figure 5 displays plots of $F_S(Q,t)$ for four time increments constructed from the van Hove functions shown in Fig. 4. The functions $F_S(Q,t)$ were calculated from $G_S(\mathbf{R},t)$ by performing the two-dimensional Fourier transform [Eq. (5.1)] numerically [18]. The data are compared to the Gaussian model prediction {solid lines: $F_S(Q,t)=\exp[-Q^2\tilde{D}_S(t)t]$} where the effective self-diffusion coefficient has been replaced with the arbitrarily chosen constant $D=1.37\times10^{-9}$ cm^{2}s^{-1}. It can be seen that, aside from the small deviations for the shortest time increment, the decays are well described as Gaussian functions of Q. Hence the first cumulant approximation [Eq. (3.14)] is a valid assumption for our system.

Figure 6 displays a direct comparison of $F(Q,t)/S(Q)=F_S(Q,t)$ determined from the EWDLS data (small circles) and from the DVM data (big circles) as a function of t for four different wave numbers. The Gaussian model prediction is also shown (solid lines). The light scattering data were obtained by numerical inversion of Eq. (4.6), while the microscopy data were calculated by the methods described in Sec. IV B. As mentioned previously, both the self and total parts of the intermediate scattering function were evaluated using the microscopic particle trajectories. Because the two were indistinguishable, only the self part of $F_S(Q,t)$ is observed in either measurement. During the manipulation of the light scattering data, it was necessary to account for residual scattered light due to background excitation apart from the evanescent wave but still associated with the incident laser beam. Scattering centers at the suspension-glass interface cause a small portion of the incident beam

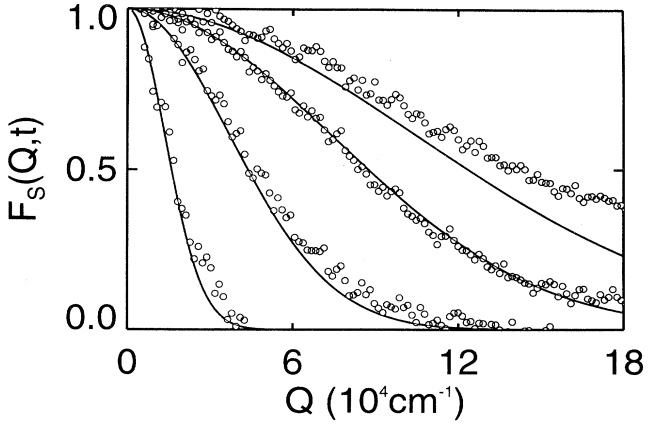

FIG. 5. Self part of the intermediate scattering function plotted against Q. The data points (circles) are calculated from the van Hove functions obtained from the displacement histograms shown in Fig. 4. The solid lines are model Gaussian functions, $\exp[-Q^2Dt]$, with $D=1.4\times10^{-9}$ cm^{2}s^{-1}. The top set of curves correspond to $t=33$ ms; subsequent sets correspond to $t=66$, 264, and 1980 ms.

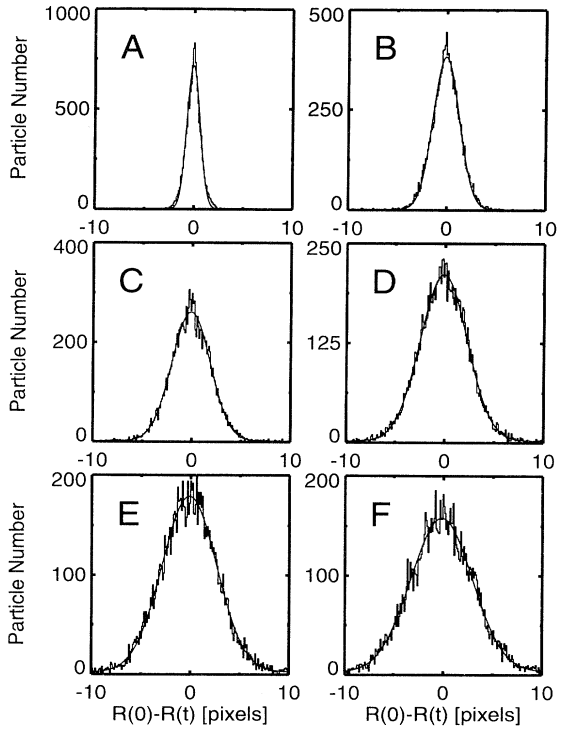

FIG. 4. Number histograms of self particle displacements in a time interval t. The smooth solid lines are least squares fit Gaussian functions with height H, offset from the origin o, and standard deviation σ. The displacements are given in units of pixels (1 pixel=0.17 μm). (A) $t=33$ ms, $H=714.2$, $o=0.06295$, and $\sigma=0.6555$; (B) $t=99$ ms, $H=379.8$, $o=0.07409$, and $\sigma=1.315$; (C) $t=198$ ms, $H=258.8$, $o=0.1096$, and $\sigma=1.938$; (D) $t=297$ ms, $H=208.3$, $o=012\,01$, and $\sigma=2.373$; (E) $t=396$ ms, $H=176.0$, $o=0.1394$, and $\sigma=2.765$; (F) $t=495$ ms, $H=154.1$, $o=0.1638$, and $\sigma=3.087$.

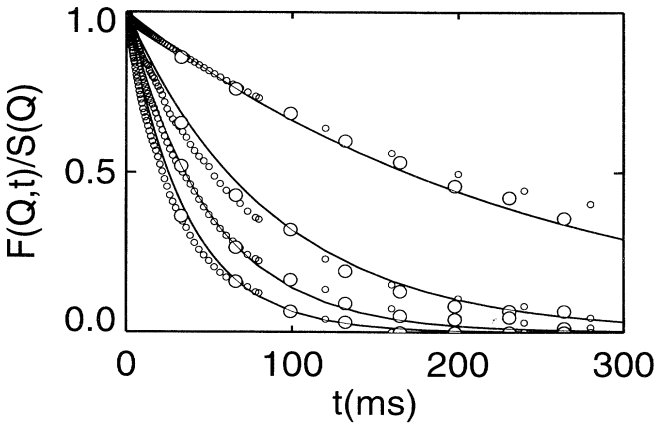

FIG. 6. Normalized intermediate scattering function plotted against time. DVM data (big circles) and EWDLS data are compared to exponential decays defined in Fig. 5 (solid lines). The top set of points correspond to $Q=54\,551$ cm^{-1}. Subsequently faster sets of decays correspond to $Q=91\,128$, 23 076, and 144 026 cm^{-1}.

to refract, leading to an anisotropic distribution of background excitation energy. This background has its largest effect at small angles. The effect was removed by dividing the scattering function by the average intensity distribution. In addition, the raw light scattering data corresponding to the smallest scattering angle ($Q = 54\,551$ cm^{-1}) displayed temporal oscillations between 0 and 100 ms due to ringing in the detection system's electronics. For this reason, a polynomial fit to the raw light scattering data, which retains the functional form of the decay while neglecting the noise, is shown for this wave vector. The polynomial was optimized to fit the data best over the range of time scales for which there is overlap with the microscopy data (10–500 ms).

We note that the agreement between the two measurements in $F_S(Q,t)$ is excellent; over the range of Q we have investigated (Table II) the time dependences of the independently determined scattering functions are in quantitative agreement. The temporal deviations from exponential behavior can be seen from the plots shown in Fig. 7. Here, the negative logarithms of the scattering functions are given as linear functions of time. The solid lines represent the Gaussian model prediction which can be compared to both the light scattering (small circles) and the microscopy data (big circles). As expected, the deviations are small, but they are discernible. Furthermore, the deviations do not appear to depend on Q.

Figures 8(a)–8(d) display $\tilde{D}_S(t)$ against $\ln t/t$ for the four wave vectors given in Table I. The temporal range displayed for each wave vector was chosen to correspond to the full decay of the intermediate scattering function (see Fig. 6). In the case of the largest scattering angles [Figs. 8(c) and 8(d)] the data points three factors of e smaller than the initial value of $F_S(Q,t)$ ($t > 150$ ms) have been omitted. The agreement and linear form are striking for all of the wave vectors studied. Because no adjustments were made to the microscopy data, least squares linear fits were made to these points alone (solid lines).

At shorter time intervals (where there is no overlap between the DVM and EWDLS measurements) the light scattering data deviate from the $(\ln t)/t$ behavior shown in Fig. 8. Between 1 μs and 5 ms, the effective diffusion coefficient appears to increase to a maximum value which occurs at approximately $t = 5$ ms. This behavior of the effective diffusion coefficient could arise from the transition from three-dimensional to two-dimensional Smoluchowski dynamics, which must occur in our system in some time range. Paul and Pusey have reported an experimental study of the time variation of the effective diffusion coefficient of a Brownian particle in a three-dimensional system [22]. For a Brownian particle with about the same diameter as that in our experiments they find that the effective diffusion coefficient approaches its asymptotic value, dressed by the hydrodynamic effects of the slowly decaying tail of the velocity autocorrelation function, on the 5–10 μs time scale. Further work is necessary to determine the nature of the short time behavior we have observed; this will be the subject of a future study.

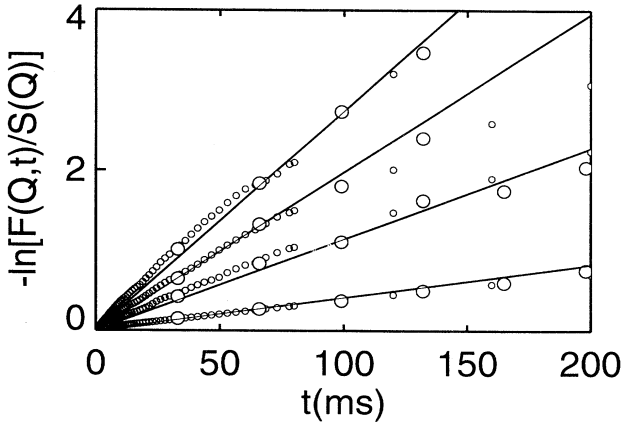

FIG. 7. Logarithmic plots of the intermediate scattering function against time. DVM data (big circles) and EWDLS data are compared to the Gaussian model defined in Fig. 5 (solid lines). The bottom set of points correspond to $Q = 54\,551$ cm^{-1}. Subsequently higher sets correspond to $Q = 91\,128$, 123 076, and 144 026 cm^{-1}.

Table III lists values obtained from the linear fits shown in Fig. 8. According to Eq. (3.5), the intercept is equal to the long time diffusion constant D_S^L, while the slope $[(D_S^S - D_S^L)\tau_L]$ is the difference between the long and short time diffusion constants scaled by the constant τ_L. The values obtained for D_S^L and $[(D_S^S - D_S^L)\tau_L]$ appear to be independent of Q with the exception of the slope for the $Q = 123\,076$ cm^{-1} data set, in which case the slope appears to be smaller by a factor of 2. The Q independence of $\tilde{D}_S(t)$ is an anticipated result since the Gaussian model has been shown to be a valid approximation for our system; hence higher-order cumulants do not significantly contribute to $F_S(Q,t)$, which is well de-

TABLE II. Time constants for 1 μm PMMA spheres in 10% aqueous sucrose. τ_f is the momentum relaxation time of fluid displaced by a particle's volume, τ_B is the relaxation time of the velocity autocorrelation function of a Brownian particle, τ_H is the hydrodynamic screening time beyond which hydrodynamic effects become important, and τ_D is the structural relaxation time.

τ_f	τ_B	τ_H	τ_D
195 ns	50 ns	81.2 μs	101 s

TABLE III. Slopes and y intercepts for $\tilde{D}_S(t)$ vs $\ln t/t$ (Fig. 8) as a function of Q.

Q (cm^{-1})	$(D_S^S - D_S^L)\tau_L$ (cm^2)	D_S^L (cm^2 s^{-1})	τ_L (s)
54 551	7.72×10^{-9}	1.15×10^{-9}	6.6
91 128	7.44×10^{-9}	1.24×10^{-9}	6.9
123 076	3.43×10^{-9}	1.23×10^{-9}	3.1
144 026	6.81×10^{-9}	1.22×10^{-9}	6.2

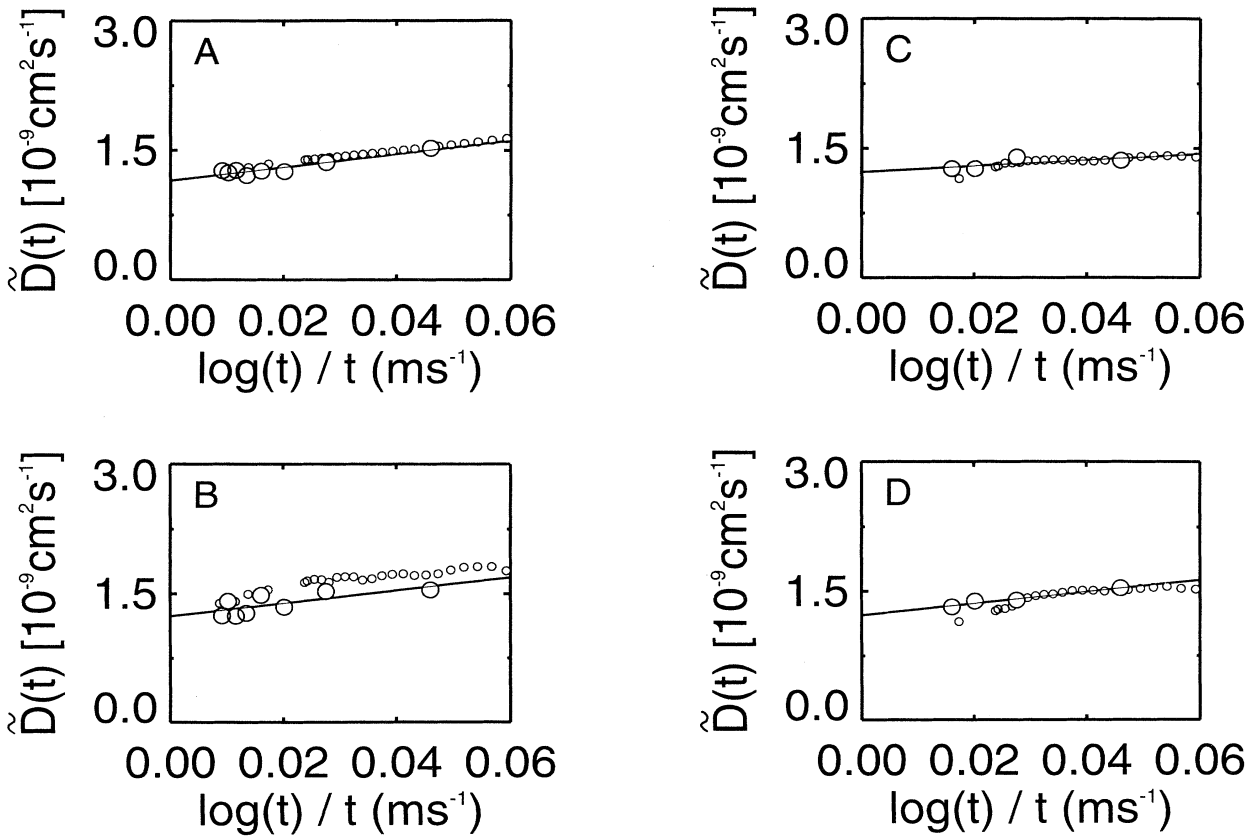

FIG. 8. The effective diffusion coefficient $\tilde{D}_S(t)$ plotted against $\ln(t/1\text{ ms})/t$. The range of time intervals covered is from 20 to 300 ms. DVM data are represented as big circles and EWDLS data are represented as small circles. The solid lines are linear least squares fits to the microscopy data. (A) $Q=54\,551\text{ cm}^{-1}$; (B) $Q=91\,128\text{ cm}^{-1}$; (C) $Q=123\,076\text{ cm}^{-1}$; (D) $Q=144\,026\text{ cm}^{-1}$. The slopes and intercepts are given in Table III.

scribed by Eq. (4.14). The spread in the observed values of D_S^L is small (standard deviation of 0.035) with an average equal to $1.21\times10^{-9}\text{ cm}^2\text{s}^{-1}$. This value of D_S^L is reached according to the form given by Eq. (3.5) over the time interval shown in Figs. 8(a)–8(d) (20 ms $< t <$ 300 ms). The short time diffusion coefficient D_S^S could nominally be assigned the same value as the bare diffusion constant, namely, $D_0=0.707k_BT/6\pi\eta a=2.32\times10^{-9}$ cm^2s^{-1}, calculated from the Stokes-Einstein equation with the necessary correction to account for the hydrodynamic friction due to the effect of the cell walls [23]. It is evident from Figs. 8(a)–8(d) that at the shortest time shown ($t=20$ ms) the diffusion coefficient has a value similar to if not somewhat smaller than our estimated D_0. Using this value for D_S^S, we calculated the time constants τ_L listed in the last column of Table III. To determine τ_M, it is necessary to take the asymptotic constant value of the difference equation [4],

$$W(t)-D_S^L t=(D_S^S-D_S^L)\tau_L\ln(t/\tau_M)\ . \tag{5.2}$$

In our current analysis, we found that the precision of our data was not sufficient to calculate a reliable value for τ_M. However, the determination of all four constants as a function of particle concentration is the topic work in progress.

For the two-dimensional Smoluchowski liquid, $\tau_L\sim a^2/D_0\cong1$ s. Thus the magnitude of the measured $(\ln t)/t$ term in Eq. (3.5) is approximately seven times larger than the theoretical prediction. Another inconsistency occurs between our data and the theoretical prediction of Ackerson and Fleishman [16]. The measured long time diffusion constant appears to overestimate the predicted concentration dependence ($D_S^L/D_S^S=[1-2\phi]=0.98$) by a factor of 24. These disagreements are larger in magnitude than the estimated statistical error in the measurements.

It is possible that the disagreement between theory and experiment is due to systematic errors. It is doubtful, however, that such errors could occur in either or both the DVM and EWDLS experiments and still lead to the observed agreement between the two measurements. Another possible source of error is the estimated value of D_0, which depends on the sucrose concentration of the host solution; that concentration is estimated to be accurate within 1%, and we presume the tabulated viscosity

of sucrose solutions has the same accuracy. Our estimate of D_0 also depends on the hydrodynamic correction due to wall effects. The wall spacing was determined to be 3 μm by visualizing defects on the walls. This measurement should have a precision of roughly the depth of focus of the objective, 200 nm, so we expect the error in the wall correction to the frictional force to be small. Although there could be an unrecognized systematic error in our measurements, we do not believe this to be the case. It is important to note that an error in D_0 alone cannot account for the discrepancies in both D_S^L/D_S^S and τ_L, since a variation in D_0 can only lead to improvement in one quantity at the expense of the other. The most probable explanation is that the idealized theoretical values obtained for the coefficients should not directly apply to our experimental system. This is not too surprising since the theoretical model is based on a strictly two-dimensional system of colliding hard disks in the absence of hydrodynamic interactions, which is certainly very different from our quasi-two-dimensional colloidal suspension.

VI. SUMMARY

We have presented experimental evidence for the time dependence of the transition of the effective diffusion coefficient in a quasi-two-dimensional suspension of hard sphere Brownian particles from the "free particle" value to the dressed particle value. For the intermediate time range ($\tau_H < t < \tau_D$) the diffusion coefficient decays from its short time "free particle" value to its dressed value as $(\ln t)/t$ in agreement with the theoretical prediction of Cichocki and Felderhof [4]. The decay of the diffusion coefficient is due to direct in-plane particle-particle collisions and is not a consequence of hydrodynamic interactions; the latter are important in determining the effective diffusion coefficient at shorter times ($\tau_B < t < \tau_H$) and are included in the "free particle" value. We have demonstrated this behavior using both EWDLS and DVM measurements, the former a probe of macroscopic particle dynamics and the latter a probe of microscopic particle dynamics. Our results indicate that the Gaussian approximation is an excellent representation of our system and that the time dependence of the mean square displacement may be obtained using Eq. (4.14). There is disagreement between our observations of the magnitude of the effect and the theoretical prediction. The observed magnitude is between three and seven times larger than that estimated. The discrepancy is most likely due to significant qualitative distinctions between the theoretical two-dimensional hard disk model and our experimental system.

ACKNOWLEDGMENTS

This research was supported by a grant from the National Science Foundation. We thank Professor David Grier and John Crocker for the image analysis software and for several fruitful discussions. We also thank Professor B. U. Felderhof for his helpful comments.

[1] B. J. Alder, D. M. Gass, and T. E. Wainwright, J. Chem. Phys. **53**, 3813 (1970).
[2] B. Cichocki and B. U. Felderhof, J. Chem. Phys. **89**, 1049 (1988).
[3] B. Cichocki and B. U. Felderhof, J. Chem. Phys. **89**, 3705 (1988).
[4] B. Cichocki and B. U. Felderhof, J. Phys. Condens. Matter **6**, 7287 (1994).
[5] L. Antl, J. W. Goodwin, R. D. Hill, R. H. Ottewill, S. M. Owens, S. Papworth, and J. A. Waters, Colloids Surf. **17**, 67 (1986); K. E. J. Barrett, *Dispersion Polymerization in Organic Media* (Wiley, London, 1975).
[6] M. Tokuyama and I. Oppenheim, Phys. Rev. E **50**, R16 (1994).
[7] J. Gao and S. A. Rice, J. Chem. Phys. **90**, 3469 (1989).
[8] B. Lin and S. A. Rice, J. Chem. Phys. **98**, 6561 (1993).
[9] B. Lin, S. A. Rice, and D. A. Weitz, Phys. Rev. E **51**, 423 (1995).
[10] P. N. Pusey and R. J. A. Tough, in *Dynamic Light Scattering: Applications of Photon Correlation Spectroscopy,* edited by R. Pecora (Plenum, New York, 1985).
[11] C. A. Murray, D. H. v. Winkle, and R. A. Wenk, J. Phys. Condens. Matter **2**, SA385 (1990).
[12] D. G. Grier and C. A. Murray, private communication.
[13] H. Lowen, J. Phys. Condens. Matter **4**, 10 105 (1992).
[14] W. Schaertl and H. Sillescu, J. Colloid Interface Sci. **155**, 313 (1993).
[15] J. C. Crocker and D. G. Grier (unpublished).
[16] B. J. Ackerson and L. Fleishman, J. Chem. Phys. **76**, 2675 (1982).
[17] B. J. Berne and R. Pecora, *Dynamic Light Scattering* (Krieger, Malabar, 1976).
[18] F. Lado, J. Comput. Phys. **8**, 417 (1971).
[19] *Handbook of Mathematical Functions,* edited by M. Abramowitz and I. A. Stegun (Dover, New York, 1964).
[20] B. Cichocki and R. B. Jones, Z. Phys. B **68**, 513 (1987).
[21] M. P. Allen and D. J. Tildesley, *Computer Simulation of Liquids* (Oxford Science, Oxford, 1987).
[22] G. L. Paul and P. N. Pusey, J. Phys. A **14**, 3301 (1981).
[23] J. Happel and H. Brenner, *Low Reynold's Number Hydrodynamics* (Kluwer, Dordrecht, 1963).

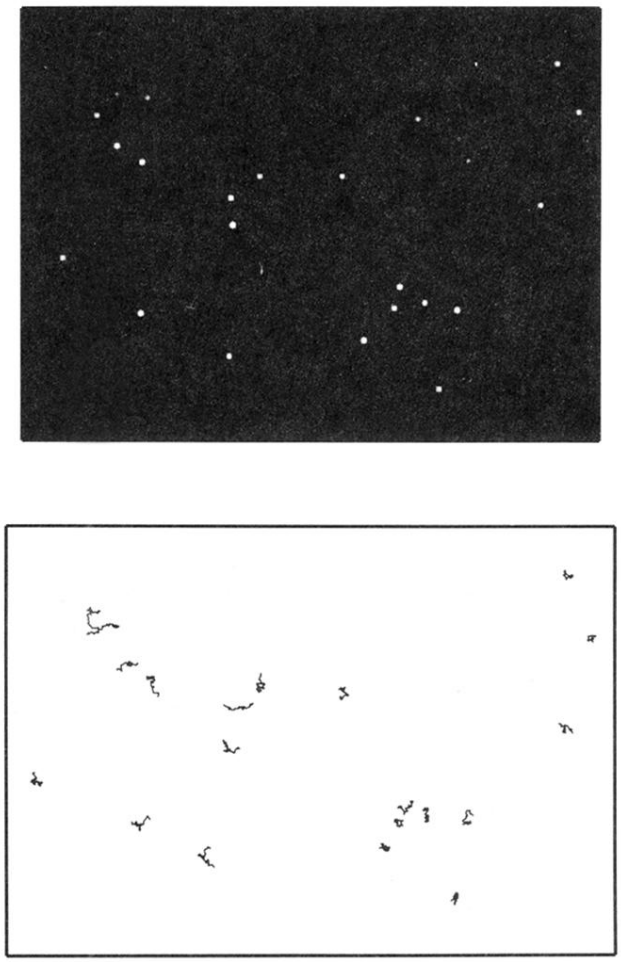

FIG. 3. Processed image of a quasi-two-dimensional colloidal suspension. The processing details are described in Sec. IV B. The two-dimensional packing density is approximately 1%. Shown below are individual center of mass particle trajectories for 30 consecutive image frames. The time interval between frames is 33 ms.